CHAPTER 9

CONCLUSIONS AND SUGGESTIONS FOR FUTURE WORK

9.1. Overall Conclusions

9.1.1. Single Component PCL Langmuir Monolayers at the A/W Interface

The nucleation and growth of PCL crystals in Langmuir monolayers presented in this thesis represent the first such observations of polymer crystallization in Langmuir monolayers at the air/water (A/W).[24] Both the growth and melting processes for PCL crystals were observed by *in situ* Brewster angle microscopy (BAM). Electron diffraction studies on Langmuir-Schaefer (LS) films suggest that the lamellar crystals are oriented with the polymer chain axes perpendicular to the substrate surface. Atomic force microscopy (AFM) studies carried out on LS-films reveal a crystal thickness of ~ 8 nm with a flat surface for what was the polymer/water interface. This value is particularly interesting when it is compared to the threshold thickness (~ 6 nm) below which dendritic growth of PCL crystals was observed in spincoated PCL films on solid substrates. For the PCL dendrites observed in spincoated systems, the polymer chains are also oriented perpendicular to the surface. As such, Langmuir film studies of PCL can provide information about crystallization phenomena that is relevant to other confined geometries. Moreover, Langmuir film studies have certain advantages: room temperature crystallization, variable pressure, fewer defects, and relatively easy sample preparation that can provide new insight into polymer crystallization.

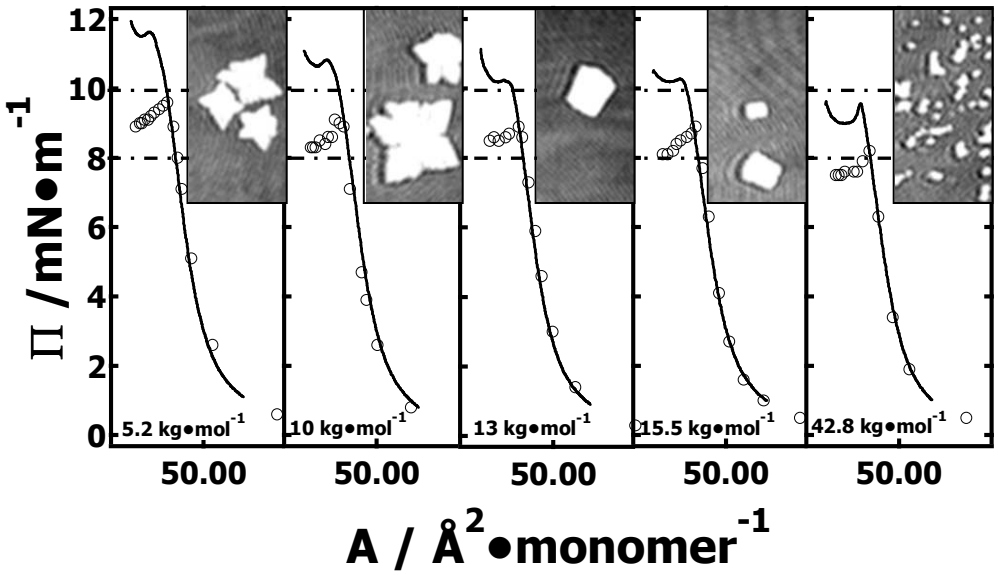

Figure 9.1. Comparisons between "equilibrium" (addition) and dynamic (compression) Π-A isotherms for PCL samples with different molar masses (M_w = 5.2, 10, 13, 15.5, and 42.8 kg·mol^{-1}). The compression isotherms (solid line) were obtained at a constant compression rate of 8 cm^2·min^{-1} and T = 22.5 °C. The circles represent successive addition data. The horizontal dashed lines at Π = 8 and 10 mN·m^{-1} are only provided to guide the eye. Detailed discussions were provided in Chapter 8.[26]

Additional findings for PCL crystallization in Langmuir film systems include the observation that the nucleation of PCL crystals occurs from meta-stable ("supercooled") monolayers just below the dynamic collapse pressures, Π_C, and above the "equilibrium collapse pressure", $\Pi_{C,e}$, as summarized for PCL samples with various molar masses in Figure 9.1. Our studies clearly indicate that the nucleation, growth, and melting of PCL crystals in Langmuir monolayers is strongly affected by PCL molar mass. The molar mass dependent growth of PCL crystals are further confirmed by average growth rate

data estimated from a series of BAM images obtained during dynamic compression experiments. A maximum growth rate observed at an intermediate weight average molar mass (M_w = 10 kg·mol^{-1}) provides evidence for a competition between lower segmental mobility and a greater degree of undercooling with increasing molar mass. The morphological study is particularly interesting, as it shows diffusion-limited growth for the lower molar mass PCL samples (M_w = 5.2 and 10 kg·mol^{-1}) and dendritic morphologies are clearly observed during expansion of these films. In contrast, for higher molar mass samples (M_w = 13, 15.5, and 42.8 kg·mol^{-1}), the diffusion of polymer chains during compression inhibits crystal growth; while the greater degree of undercooling favors nucleation leading to more and smaller crystals.

9.1.2. PCL-Based Polymer Blends as Langmuir Films at the A/W Interface

Two different binary PCL-based blends were used to explore the phase behavior of polymer blends with different compatibility in Langmuir films at the A/W interface. For PCL (M_w = 10 kg·mol^{-1}) and poly(t-butyl acrylate) (PtBA, M_w = 25.7 kg·mol^{-1}) blends, thermodynamic analyses of Π-A isotherms reveal that PCL/PtBA blends are compatible as Langmuir films below the dynamic collapse pressure, Π_C ~ 11 mN·m^{-1}, for the PCL component. For PCL-rich blends, *in situ* BAM studies reveal nonequilibrium growth of PCL dendritic crystals for compression past the PCL collapse transition. PCL crystals grown in the plateau regime of the Π-A isotherm exhibit dendritic morphologies. These diffusion-limited structures presumably arise from the exclusion of PtBA from the growing PCL crystals and hindered diffusion of PCL from the surrounding monolayer to the crystal growth fronts. AFM also reveals that the polymer/water crystal surface is very flat and the crystal thickness of PCL dendrites is ~ 7 to 8 nm, which is comparable

to PCL crystals grown from single-component PCL monolayers. In contrast, PCL crystallization is suppressed in PtBA-rich blend films.

Morphological evolution of PCL dendrites for a representative PCL/PtBA blend with a PtBA mole fraction of $X_{PtBA} \sim 0.14$ were further examined under various experimental conditions. Dynamic compression experiments performed at various compression rates revealed smaller dendritic crystals at similar surface area per monomer at higher compression rates. Nevertheless, the average growth rate analyses yield similar growth rates, leading to the conclusion that the size of crystals grown at different compression rates is a function of the growth time rather than compression rate. By switching from a constant compression rate experiment to an isobaric area relaxation experiment at different Π, it was possible to show that dendritic morphologies depended on Π. From high Π to low Π, there was a series of transitions from highly branched symmetric dendrites, to six-arm dendrites, four-arm dendrites, seaweedlike crystals, and distorted rectangular crystals. In isobaric area relaxation experiments, Π is analogous to temperature in bulk isothermal crystallization studies and has a profound impact on morphological selection because of the interplay between diffusion, interfacial energy, and the anisotropy of the interfacial energy.

In contrast, PCL (M_w = 10 kg·mol^{-1}) and glassy polystyrene (PS) with molar masses of M_w from 1.56 to 217 kg·mol^{-1} are immiscible as Langmuir films at the A/W interface.[25] Surface pressure-average area per monomer, Π–<A>, analyses indicate that the surface concentration of amphiphilic PCL is the only factor influencing the surface pressure below the collapse transition. For PS-rich blends, *in situ* BAM studies at the A/W interface and AFM studies on LS-films reveal that PS nanoparticle aggregates formed at

very low surface pressures can form networks upon further compression. The morphologies seen in PS-rich blends (networklike rings) suggest that the nonamphiphilic PS aggregates at the A/W interface produce domains with dipole densities that differ from that of pure PCL. In all composition regimes, the amphiphilic PCL phase tends to spread and form a continuous surface layer at the A/W interface, while simultaneously improving the dispersion of nonamphiphilic PS domains. For PCL-rich blends, compressing the blend films past Π_C for the PCL component leads to the nucleation and growth of PCL crystals around small PS aggregates. In this case, these small PS aggregates act as heterogeneous nucleation centers for the growth of PCL crystals, which has been further confirmed by the morphologies captured by BAM during expansion experiments. During film expansion, BAM images show a gradual change in the surface morphology from highly continuous networklike structures (PS-rich blends) to broken ringlike structures (intermediate composition) to small discontinuous aggregates (PCL-rich blends). In comparison to PCL/glassy PS blends, preliminary BAM results obtained from PCL/liquid PS oligomer blends as Langmuir films at the A/W interface have entirely different morphologies and may exhibit "liquid-liquid" phase separation.

In conclusion, results and discussion for PCL and PCL-based polymer blends presented in Chapters 4 through 8 demonstrate clear evidence that polymeric Langmuir monolayers at the A/W interface can be considered as a superb model system for studying the physical transformations of polymers confined to 2D geometries, including crystallization and phase separation. The extensive studies covered in this thesis provide significant supplements to the field of traditional polymer physics, particularly for polymer crystallization.

9.2. Suggestions for Future Work

9.2.1. Effects of PtBA Molar Mass on the Morphologies of PCL Dendrites

As shown in Chapter 5, a weakly composition dependent morphological transition has been observed for PCL dendrites grown in various PCL/PtBA blends, although a quantitative discussion of the diffusive properties as a function of PtBA composition is not possible at the current time because of a lack of experimental diffusion data. In any event, PtBA molar mass can serve as another important factor for controlling the dendritic sidebranching during the formation of PCL dendrites in compression experiments at a constant rate. The diffusion coefficient of PtBA homopolymers decreases with increasing PtBA molar mass as $\sim M^{-2}$. As a result, increasing PtBA molar mass may alter the morphologies of PCL dendrites in the blends by changing the effective diffusion coefficients in the system. AFM images obtained from PCL (M_w = 10 kg·mol^{-1})/PtBA (M_w = 39.2 kg·mol^{-1}) with PtBA mole fraction of $X_{PtBA} \sim 0.40$ are shown in Figure 9.2. These preliminary results indicate that the dendritic branches observed for this sample are very similar to the results observed for a $X_{PtBA} \sim 0.44$ PCL (M_w = 10 kg·mol^{-1})/PtBA (M_w = 25.7 kg·mol^{-1}) blend. The average crystal thickness is also about 7.5 nm. One should note that a relatively small change of PtBA molar mass from 23.8 kg·mol^{-1} to 37 kg·mol^{-1} may not lead to a dramatic change of the diffusion coefficient. Therefore, PtBA samples with much shorter chain lengths, such as a PtBA sample with $M_w \sim 5$ kg·mol^{-1}, should be considered to further study the effects of matrix molar mass on the dendritic morphologies of PCL dendrites. For PtBA samples with such a low molar mass, the rejection process of PtBA chains from PCL crystals could become much faster because of a higher diffusion coefficient, possibly leading to more fully filled PCL

dendrites. One sample optical microscopy (OM) image obtained from a representative blend of PCL (M_w = 10 kg·mol^{-1})/PtBA (M_w = 15 kg·mol^{-1}) with X_{PtBA} ~ 0.20 is shown in Figure 9.3. Some of PCL dendrites clearly show more fully filled centers in comparison to PCL blends with higher molar mass PtBA. Meanwhile, more irregular sidebranching, presumably in the {100} sectors, was observed. These preliminary results clearly show that variation of molar mass of PtBA may not only affect the growth rate but could also affect the selection of sidebranches and the gross morphologies of PCL dendrites. More detailed studies of this subject will provide greater insight into the influence of how matrix mobility affects morphological selection of PCL dendrites. Moreover, direct measurements of PCL and/or PtBA should be possible by fluorescence recovery after photobleaching (FRAP). Additionally PCL/PtBA blends would be ideal for surface light scattering (SLS) studies. SLS provides the dynamic dilational surface elasticity. Together SLS and FRAP studies would be an ideal way to quantify changes in fluidity with composition and molar mass.

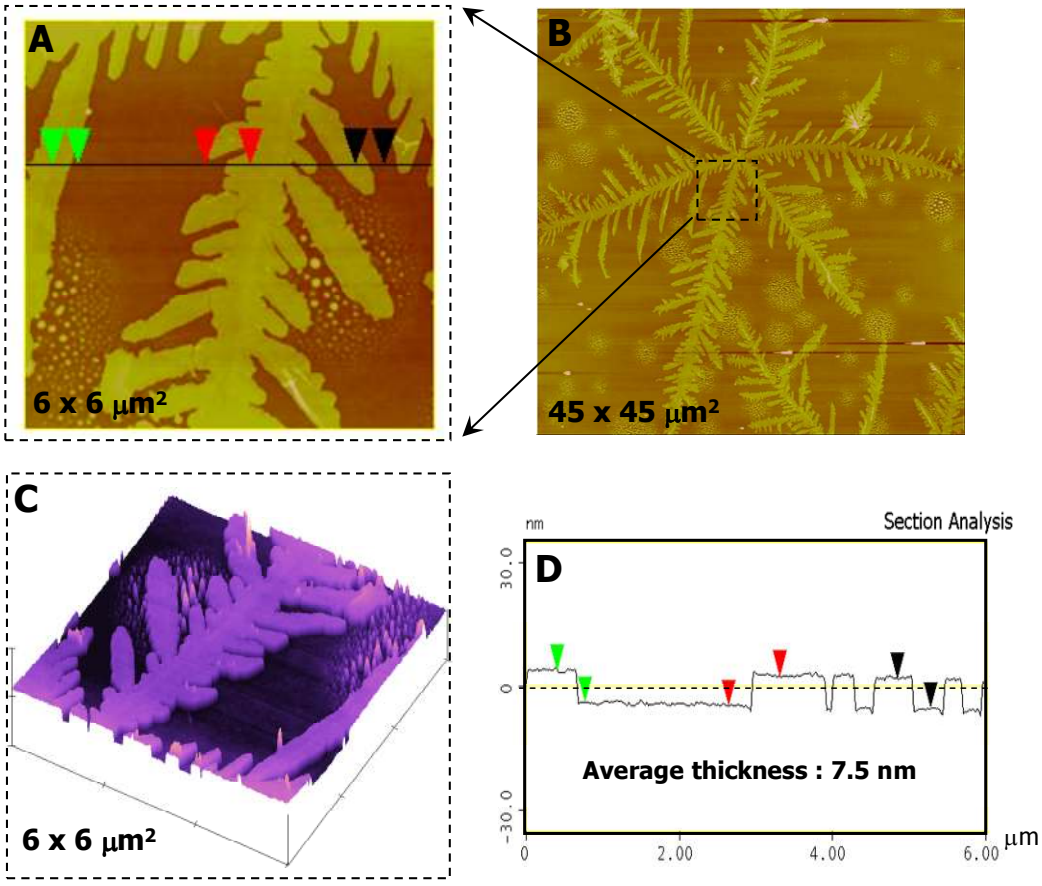

Figure 9.2. AFM images of a single layer LS-film for a representative X_{PtBA} ~ 0.40 PCL(M_w = 10 kg·mol^{-1})/PtBA (M_w = 39.2 kg·mol^{-1}) blend. The LS-film was transferred onto a PS coated silicon substrate at Π ~ 11 mN·m^{-1} in the plateau regime during compression. (A) a 6 × 6 μm^2 height image; (B) a 45 × 45 μm^2 height image. The dendritic branches shown in the dashed box of (B) corresponds to image (A); (C) a 6 × 6 μm^2 three dimensional image corresponding to image (A); (D) a cross-sectional analysis for the solid line in (A). The average thickness of the lamellar crystals is ~ 7.5 nm. Z-scales for images A and B are 0 to 80 nm. The z-scale for C is 40 nm.

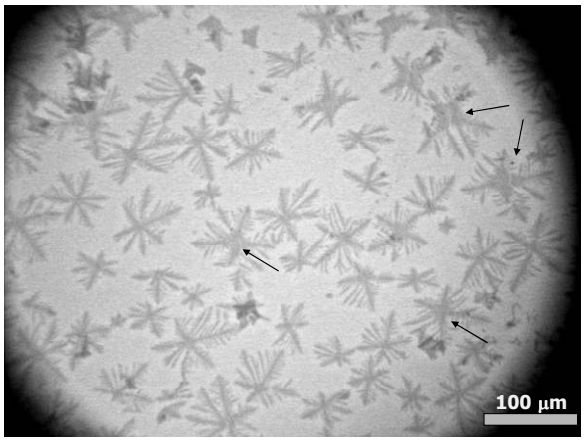

Figure 9.3. A representative OM image of a single layer LS-film prepared from a representative X_{PtBA} ~ 0.20 PCL (M_w = 10 kg·mol^{-1})/PtBA (M_w = 15.3 kg·mol^{-1}) blend. The LS-film was transferred onto a PS coated silicon substrate in the plateau regime during compression. Some crystals show more fully filled centers as indicated by the arrows.

9.2.2. Variation of the PCL Molar Mass

The molar mass dependent growth of PCL crystals in single-component Langmuir monolayers has been studied and discussed in Chapter 8. Both the growth rate and crystal morphologies were found to vary with PCL molar mass. Preliminary AFM results obtained from a single layer LS-films transferred for a X_{PtBA} ~ 0.30 PCL (M_w = 15 kg·mol^{-1})/PtBA (M_w = 39.2 kg·mol^{-1}) blend are shown in Figure 9.4. Figure 9.5 shows AFM images obtained from LS-films transferred for a X_{PtBA} ~ 0.20 PCL (M_w = 42.8 kg·mol^{-1})/PtBA (M_w = 39.2 kg·mol^{-1}) blend. Figures 9.4 and 9.5 clearly show that dendritic growth of PCL crystals occurs throughout the examined molar mass range from M_w = 10 to 42.8 kg·mol^{-1}.

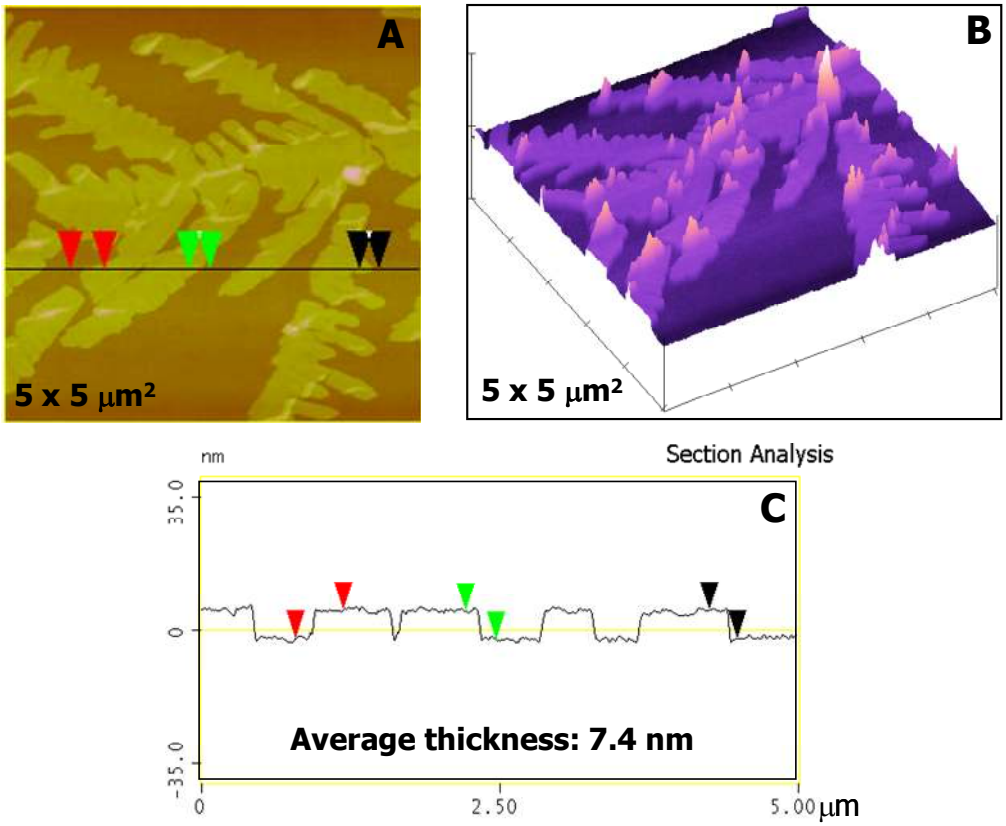

Figure 9.4. AFM images of a representative single layer LS film for a X_{PtBA} ~ 0.30 PCL (M_w = 15.5 kg·mol^{-1})/PtBA (M_w = 39.2 kg·mol^{-1}) blend. The LS film was transferred onto a PS coated silicon substrate in the plateau regime after Π_C during compression. (A) a 5 × 5 μm^2 height image; (B) a 5 × 5 μm^2 three dimensional image corresponding to image (A); (C) a cross-sectional analysis for the solid line in (A). The average thickness of the lamellar crystals is 7.4 nm. Z-scales for images A and B are 0 to 60 nm.

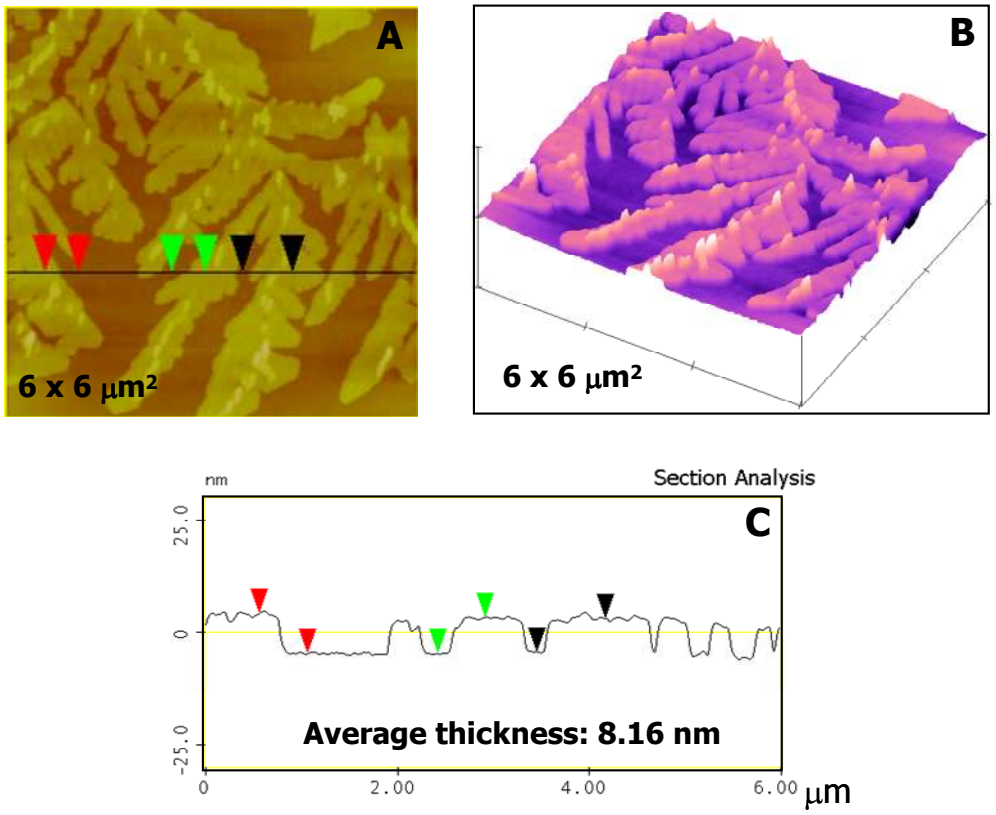

Figure 9.5. AFM images of a representative single layer LS film for a X_{PtBA} ~ 0.20 PCL (M_w = 42.8 kg·mol^{-1})/PtBA (M_w = 39.2 kg·mol^{-1}) blend. The LS film was transferred onto a PS coated silicon substrate in the plateau regime after Π_C during compression. (A) a 6 × 6 μm^2 height image; (B) a 6 × 6 μm^2 three dimensional image corresponding to image (A); (C) a cross-sectional analysis for the solid line in (A). The average thickness of the lamellar crystals is 8.5 nm. Z-scales for images A and B are 0 to 60 nm.

In contrast to the PCL dendrites discussed in Chapters 5 and 6, AFM results clearly show fewer and more irregular sidebranches are observed for the higher molar mass PCL samples (M_w = 15.5 and 42.8 kg·mol^{-1}), suggesting a greater degree of undercooling and a lower segmental mobility with increasing molar mass may affect both the anisotropy of the interfacial tension and the magnitude of the compositional fluctuations during crystallization. Further studies of molar mass dependent growth of dendritic PCL crystals such as growth rate analyses, measurements of the degree of sidebranching from the dendritic trunks, melting behavior of crystals, etc. will provide tremendous information for understanding how changing the diffusion field alters crystal morphology in blends at surface. Coupling these studies with SLS and FRAP measurements will provide important quantitative details about thin film fluidity relative to morphological features.

9.2.3. Growth Mechanism for PCL Dendrites during Isobaric Area Relaxation Experiments

The nucleation and growth theory reported by Vollhardt *et al.* is a 2D analog to the 3D model developed by Avrami. Vollhardt's *et al.*'s model was specially developed for homogeneous nucleation of three dimensional (3D) small molecular domains with nucleation centers that are assumed to have simple geometrical shapes.[67-69] The generalized expression of a nucleation and growth model for 3D domains of small molecules at the A/W interface is given by:

$$z = \frac{A_0 - A(t)}{A_0 - A_\infty} = 1 - \exp[-K_x (t - t_i)^x] \qquad (9\text{-}1)$$

$$A(t) = A_\infty + (A_0 - A_\infty)\exp[-K_x(t - t_i)^x] \quad (9\text{-}2)$$

In Eqs. 9-1 and 9-2, A(t) is the apparent area per molecule at time t, A_0 is the initial area per molecule, and A_∞ is the apparent area per molecule as $t \rightarrow \infty$. An induction time, t_i, is introduced as a theoretical description of time dependent growth rates. Positive t_i values indicate that the growth rate at the initial stage of nucleation is smaller than the normal value for the subsequent growth process, while negative t_i values suggest a higher growth rate during the early stages of nucleation. K_x is an overall transformation rate constant that encompasses the nucleation rate k_n and growth rate k. The exponent x is different for different nucleation mechanisms and nucleation center geometries (Table 2.1).[67-69]

Vollhardt's model has been successfully applied to the study of 3D domains grown in trisilanolcyclohexyl-POSS at the A/W interface.[48(f)] In order to apply Volhardt's model, "homogeneous spreading" conditions were created and it was verified that they were significantly different from "heterogeneous spreading" conditions.[48(f)] In contrast, previous results obtained for PCL crystals grown from single-component PCL Langmuir monolayers during isobaric area relaxation experiments have shown that the application of this model to the PCL system is limited by two factors:

I) The nucleation and growth model was developed for homogeneous nucleation of small molecules. Nucleation of polymers has similarities to small molecules except that the critical nucleus involves a number of chain segments rather than a collection of molecules. In general, the homogeneous nucleation of polymers does not occur easily since the formation of a critical nucleus is energetically unfavorable. Moreover, nucleation for these polymeric systems in quiescent states is usually believed to be heterogeneous. At the A/W interface, Π can play a critical role for overcoming the

energy barrier for the formation of critical nuclei. The nucleation of PCL crystals can occur at any Π value in the supersaturated monolayer regime and the following plateau regime; however, it is safe to conclude that most nuclei are developed before or at monolayer collapse based on our observations. Nevertheless, our observations do not provide any conclusive evidence for homogeneous nucleation of PCL crystals during dynamic compression or isobaric area relaxation experiments. Thus, the assumption of homogeneous nucleation, the foundation of Vollhardt model, may not be appropriate for the PCL system.

II) The model was developed with the assumption of either hemispherical or cylindrical 3D nucleation centers, which grow in a shape-preserving fashion. Thus, the growth mechanism of 3D domains interpreted by the Vollhardt theory is dramatically simplified by considering that the area relaxation during isobaric area relaxation experiments is only caused by the growth of 3D domains with uniform size and geometry. These simplifications also imply that the growth rate of these domains is essentially linear. However, the nucleation and growth process in the PCL system reveals anisotropic crystal shapes as discussed in Chapters 4 and 8. The geometry of the 3D centers for the growth of PCL crystals is not hemispherical or cylindrical in shape. Therefore, the geometrical centers assumed by this model are over-simplified.

Isobaric area relaxation results obtained for a representative $X_{PtBA} \sim 0.14$ PCL (M_w = 10 kg·mol^{-1})/PtBA (M_w = 25.7 kg·mol^{-1}) blend were further examined by the Vollhardt model. As pointed out by Vollhardt *et al.*, only the concave-downward part of the initial relaxation curve is suitable for deducing the mechanism for the transformation of monolayer materials to the 3D collapsed phase.[67-69] Thus, only the isobaric area

relaxation curves obtained at Π = 11 and 10.5 $mN \cdot m^{-1}$ are to be considered here for fitting experimental results with the Vollhardt model as lower Π gives curves lacking clear concave-downward features. The average surface area,<A(t)> versus relaxation time, t, plots presented in Figure 9.6 only exhibit a small concave-downward shape during the initial relaxation for both Π. Meanwhile, the two relaxation curves have not flattened out by the end of the experiments. As a result, the $<A>_\infty$ parameter may have a substantial error. To solve this problem, a larger trough should be used to perform isobaric area relaxation experiments in the future.

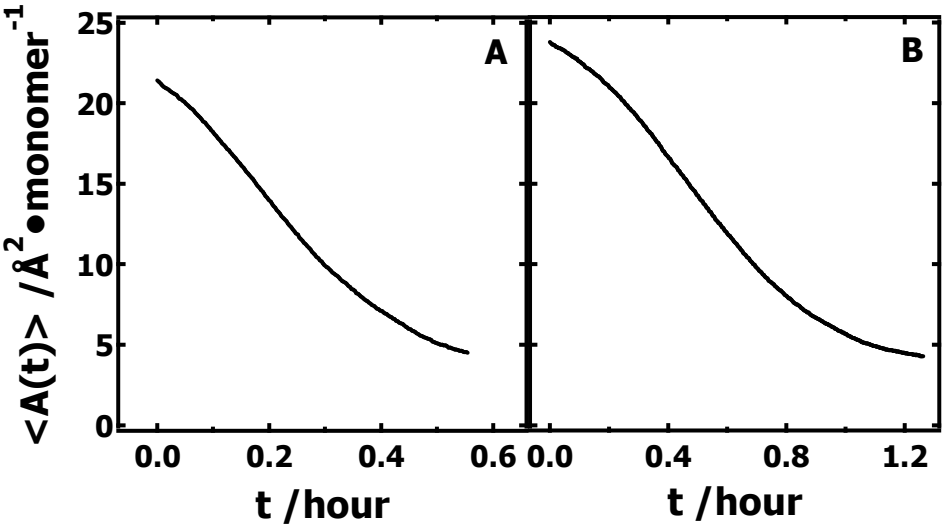

Figure 9.6. <A(t)>-t plots for representative X_{PtBA} ~ 0.14 PCL (M_w = 10 $kg \cdot mol^{-1}$)/PtBA (M_w = 25.7 $kg \cdot mol^{-1}$) blends at T = 22.5 °C during isobaric area relaxation experiments at Π values of (A) 11 and (B) 10.5 $mN \cdot m^{-1}$. As Π decreases, the area relaxation process takes longer time. <A(t)>-t plots shown here are far from flattening out to clearly show $<A>_\infty$.

Figure 9.7 shows the fitting results of experimental data with Vollhardt's model according to Eq. 9-2. The fitting results with one standard deviation error bars for the best fit are summarized in Table 9.1. For PCL dendrites grown during isobaric area relaxation experiments at $\Pi \sim 11$ mN·m^{-1}, the best fit to the experimental data provides an exponent of $x = 1.77 \pm 0.06$ and an overall transformation rate constant, $K_x = (6.68 \pm 0.18)\ h^{-1/1.77}$. As seen in Table 9.1, the best fit for dendritic growth of PCL crystals at $\Pi \sim 10.5$ mN·m^{-1} may suggest a progressive nucleation with hemispherical edge growth with exponent of $x = 2.44 \pm 0.06$ ($x \sim 2.5$) and $K_x = (1.54 \pm 0.08)\ h^{-1/2.34}$. The fitting results can also be presented in a linear fashion by converting Eq. 9-1:

$$\left[\ln\left(\frac{1}{1-z}\right)\right]^{1/x} = K_x^{1/x}(t - t_i) \tag{9-3}$$

The corresponding linear fitting results of $[\ln(1/(1-z)]^{1/x}$ vs. t are shown in the insets of Figure 9.7A and B. Although the numerical results obtained from fitting the isobaric area relaxation data with the Vollhardt model seem reasonable, the conclusions drawn for the geometries of growing 3D phase are speculative at best. Based on the extensive morphological studies discussed in Chapters 5 and 6, the highly complicated morphological features of PCL dendritic crystals can not be oversimplified as they do not grow in a shape-preserving fashion. Furthermore, it is also clear that the growth rate of dendritic sidebranches in the {100} sectors is different from {110} sectors, and that sidebranches grown along the same dendritic trunk also show a distribution of growth rates.

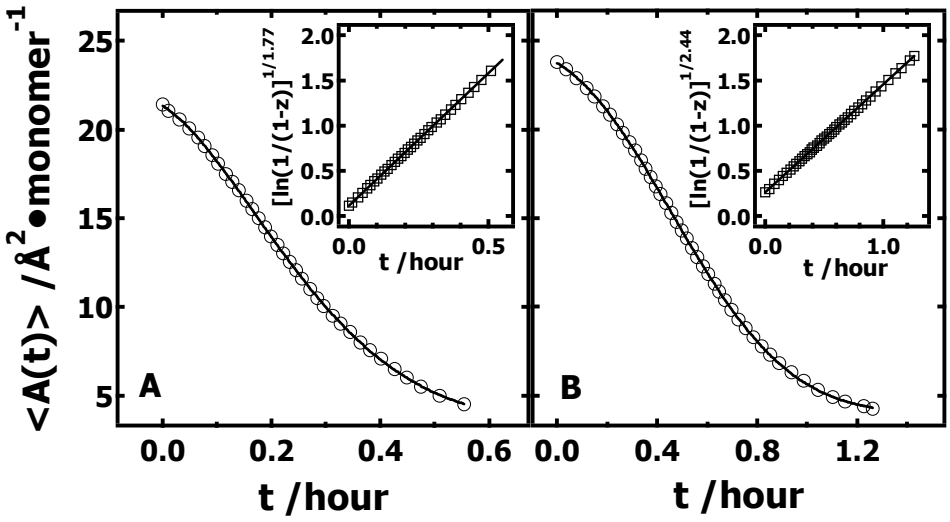

Figure 9.7. <A(t)>-t plots for representative X_{PtBA} ~ 0.14 PCL (M_w = 10 kg·mol^{-1})/PtBA (M_w = 25.7 kg·mol^{-1}) blends at T = 22.5 °C during isobaric area relaxation experiments: (A) 11 (open circles) and (B) 10.5 mN·m^{-1} (open circles). Solid lines represent the best fitting results for <A(t)>-t plots with the Vollhardt model. The solid line in the inset represents a linear representation of the data according to Eq. 9-3 using the parameters obtained from the best-fitting results of <A(t)> vs. t according to Eq. 9-2.

Table 9.1. Coefficients obtained from fitting the isobaric area relaxation experiments for representative X_{PtBA} ~ 0.14 PCL (M_w = 10 kg·mol^{-1})/PtBA (M_w = 25.7 kg·mol^{-1}) blends at T = 22.5 °C at Π values of 11 and 10.5 mN·m^{-1}accoridng to Eq. 9-2.

Π[a]	A_0[b]	A_∞[b]	K_x[c]	t_i[d]	x
11	21.84 ± 0.18	3.26 ± 0.12	6.68 ± 0.18	-0.04 ± 0.01	1.77 ± 0.06
10.5	24.50 ± 0.11	3.93 ± 0.04	1.54 ± 0.08	-0.22 ± 0.02	2.44 ± 0.06

Units: [a] mN·m^{-1}; [b] Å^2·monomer^{-1}; [c] h$^{-1/x}$; [d] h. Error bars represent ± one standard deviation.

In conclusion, these preliminary results suggest that similar limitations for applying Vollhardt's model to single-component PCL systems are also present for the dendritic growth of PCL crystals in PCL/PtBA blends. More critical experiments for future studies of PCL crystallization are needed to obtain accurate growth rate data of dendritic fingers and relate the growth rate information to the surrounding diffusion field. This information would facilitate a quantitative discussion of the factors that influence the growth mechanism of PCL dendrites. Summing the discussion thus far, the previously developed model for explaining nucleation and growth behavior at the A/W interface will need to be refined to more accurately interpret results from isobaric crystallization experiments with polymeric systems.

9.2.4. A Tentative Phase Diagram for PCL/Liquid PS Oligomer Blends as Langmuir Films

Unlike PCL blends with glassy PS, preliminary BAM studies performed for PCL/liquid PS oligomer blends as Langmuir films show interesting morphologies during multiple hysteresis experiments. In this system, both PCL crystallization and phase separation appear to be induced by compressing the blend films through various critical Π values, analogous to characteristic temperatures for the binodal and spinodal lines of a classical temperature vs. composition (T-ϕ) phase diagram.[85-89]

Figure 9.8 contains Π–<A> isotherms for PCL blends with liquid PS oligomer at various mole fractions of PS, X_{PS}. X_{PS} values are calculated on the basis of the molar masses of the repeating units rather than the molar masses of the entire polymer chains. The inset of Figure 9.8 shows Π–A isotherms for single-component PS and PCL Langmuir films at the A/W interface. The inset clearly shows PS is nonamphiphilic.

Examination of Figure 9.8 indicates that a new phase transition appears at Π below Π_C ~ 11 $mN \cdot m^{-1}$ for single-component PCL films. To accurately determine the position of this new phase transition regime, the static elasticity, $\varepsilon_{s,}$, is deduced from Π–<A> isotherms and plotted as a function of <A> as shown in Figure 9.9. In Figure 9.9A, the maximum ε_s for the PCL component at a characteristic Π_{PCL} value of ~ 6 $mN \cdot m^{-1}$ is labeled as $\varepsilon_{s,\,max,\,PCL}$, corresponding to the point where the PCL chains presumably start to fold-up and leave the A/W interface.

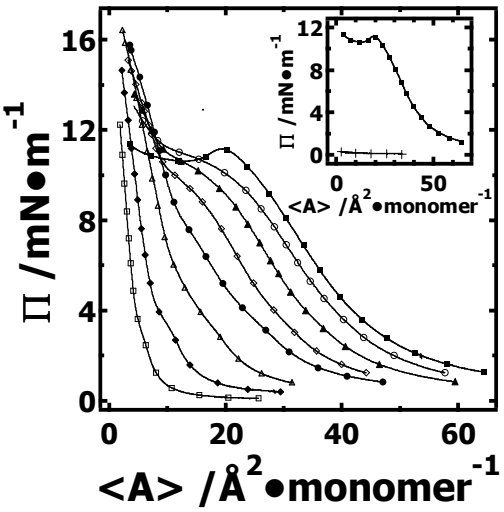

Figure 9.8. Π–<A> compression isotherms for various PCL (M_w = 10 kg•mol^{-1}) /PS (M_w = 0.74 kg•mol^{-1}) blends at the A/W interface. The isotherms were obtained at T = 22.5 °C and a compression rate of 20 $cm^2 \cdot min^{-1}$ during the 1st compression step and correspond to X_{PS} = 0 (PCL, ■), 0.13 (○), 0.22 (▲), 0.33 (◊), 0.53 (●), 0.68 (Δ), 0.77 (♦), and 0.89 (□). The inset shows Π–A compression isotherms for single component PCL (○) and PS (+) at the A/W interface. Unlike higher molar mass PS, where rigid PS domains can cause an apparent Π through mechanical perturbation of the Wilhelmy plate, Π ~ 0 at all A for the liquid PS oligomer.

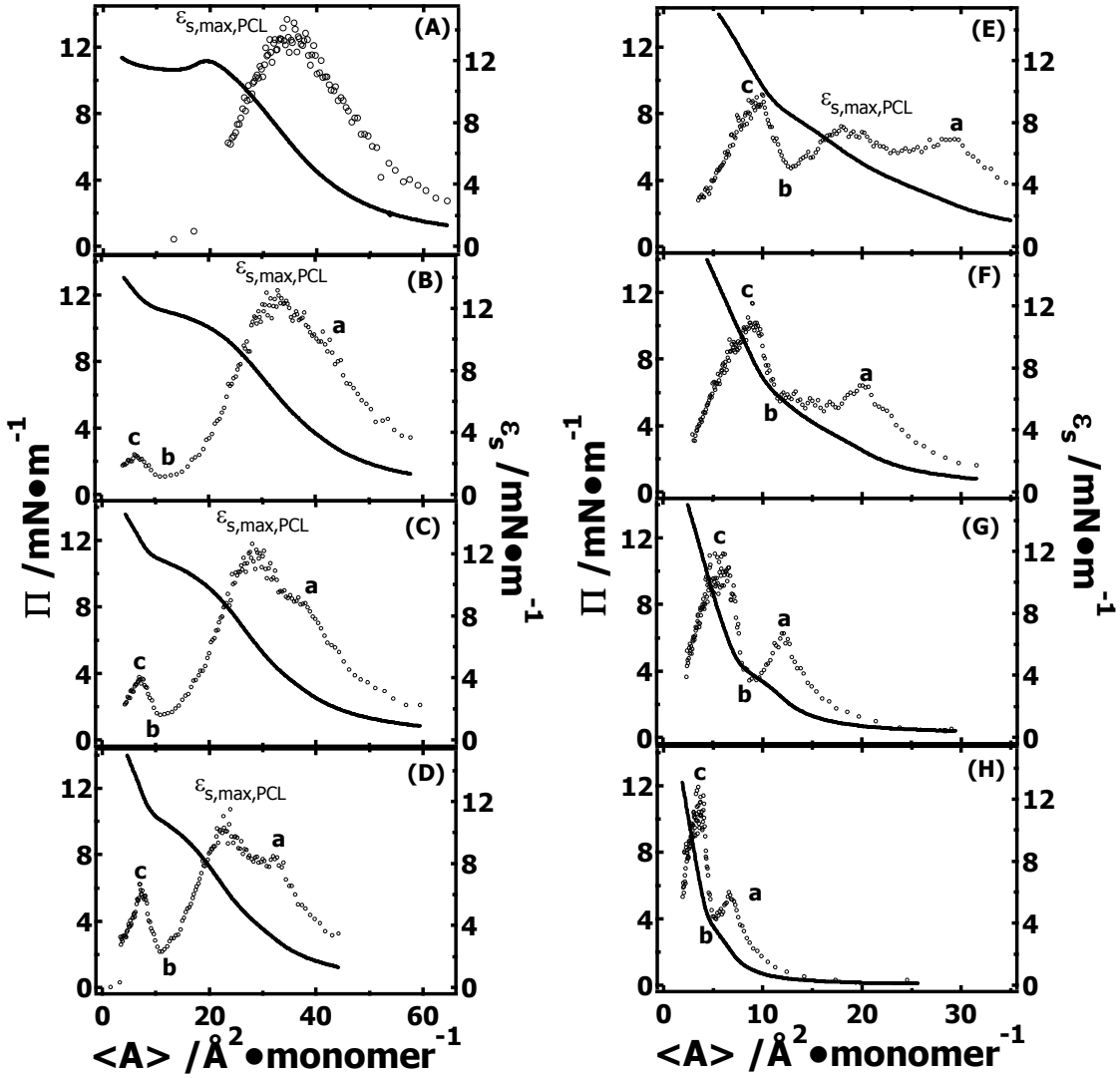

Figure 9.9. Π (left-hand axis) and ε_s (right-hand axis) versus <A> plots for various PCL (M_w = 10 kg•mol^{-1})/liquid PS oligomer (M_w = 0.74 kg•mol^{-1}) blends at the A/W interface. All isotherms were obtained at T = 22.5 °C and a constant compression rate of 20 cm^2·min^{-1} during the 1st compression step and correspond to X_{PS} = 0 (A), 0.13 (B), 0.22 (C), 0.33 (D), 0.53 (E), 0.68 (F), 0.77 (G), and 0.89 (H). Π–<A> isotherms are represented by the solid lines and the static elasticity, ε_s, is represented by the symbols (○). The letters in the figures indicate various $\varepsilon_{s,\,max}$ and $\varepsilon_{s,\,min}$ observed in the blends. Their numerical values are summarized in Table 9.2.

For Figure 9.9B through E, PCL-rich blends, there are three maxima, $\varepsilon_{s,\,max,\,a}$, $\varepsilon_{s,\,max,\,PCL}$, and $\varepsilon_{s,\,max,\,c}$ at Π_a, Π_{PCL}, and Π_c, respectively. There is also one minimum, $\varepsilon_{s,\,min,\,b}$, located at Π_b. Here, we only concern ourselves with $\varepsilon_{s,\,min,\,b}$ for $\Pi > \Pi_{PCL}$ or when Π_{PCL} is no longer evident. For PS-rich blends, there are only two maxima and one minimum, $\varepsilon_{s,\,max,\,a}$, $\varepsilon_{s,\,min,\,b}$, and $\varepsilon_{s,\,max,\,c}$ at Π_a, Π_b, and Π_c, respectively. $\varepsilon_{s,\,max,\,a}$ indicates a new transition in the monolayer regime for PCL/PS blends, corresponding to a critical Π_a, which is less than $\Pi_{PCL} \sim 6$ mN·m^{-1} for all examined PCL/PC blends. At $\Pi < \Pi_a$, the PCL/PS monolayers are relatively stable and this has been defined as Regime I. In contrast, $\Pi > \Pi_a$ likely represents the case where PS chains start to be squeezed out of the blend films because of their greater hydrophobicity than PCL chains and the tendency of PS to form a dewet layer on PCL for hydrophilic substrates.[194] Furthermore, $\varepsilon_{s,\,min,\,b}$ is used to indicate the end of this metastable monolayer regime, corresponding to a critical Π_b. The regime between Π_a and Π_b has been defined as metastable regime II and may represent the nucleation and growth of a new phase. For PCL-rich blends as seen in Figure 9.9A through E, Π_{PCL} of ~ 6 mN·m^{-1} lies inbetween Π_a and Π_b. Meanwhile, for PS-rich blends, the characteristic $\varepsilon_{s,\,max,\,PCL}$ appears to disappear as seen in Figure 9.9 F through H. Whether Π_{PCL} disappears or has been replaced by Π_c ($\varepsilon_{s,\,max,\,c}$) remains unclear. The region between Π_b and Π_c is defined as Regime II'. For $\Pi > \Pi_c$, another region is defined as Regime III. All critical Π values are further converted to surface tension, γ, as given by $\gamma = \gamma_0 - \Pi$, where $\gamma_0 = 72$ mN·m^{-1} for water at 22.5 °C. The critical ε, Π, and γ values determined for various PCL/PS oligomer blends are listed in Table 9.2.

Table 9.2. Critical ε, Π, and γ values determined for various PCL/liquid PS oligomer blends as Langmuir films deduced from Figure 9.9 for T = 22.5 °C. Lowercase letters a, b, and c are indicated in the ε_s–<A> plots in Figure 9.9. The data inside the dotted box indicates ambiguity over whether Π_{PCL} disappears or has been replaced by Π_c ($\varepsilon_{s,\,max,\,c}$).

		PCL			**a**			**B**			**C**		
	X_{PS}	ε_s	Π	γ	$\varepsilon_{s,a}$	Π_a	γ_a	$\varepsilon_{s,b}$	Π_b	γ_b	$\varepsilon_{s,c}$	Π_c	γ_c
		$mN{\cdot}m^{-1}$			$mN{\cdot}m^{-1}$			$mN{\cdot}m^{-1}$			$mN{\cdot}m^{-1}$		
A	0	14.0	6.0	66.0									
B	0.13	13.2	5.8	66.2	10.4	3.3	68.8	1.2	11.0	61	2.6	12.2	59.8
C	0.22	12.6	6.0	66.0	9.2	3.2	68.8	1.6	10.8	61.2	4.1	12.1	59.9
D	0.33	11.0	5.9	66.1	8.5	3.1	68.9	2.3	10.1	61.9	6.0	12.0	60
E	0.53	7.8	5.8	66.2	6.9	2.7	69.3	5.0	7.9	64.1	9.6	10.3	61.7
F	0.68				6.8	2.5	69.6	6.0	5.8	66.2	12.1	8.1	63.9
G	0.77				6.7	2.3	69.7	3.7	3.9	68.1	12.0	6.4	65.6
H	0.89				6.0	2.0	70	4.4	3.6	68.4	12.4	5.2	66.8

The critical γ values are plotted as a function of X_{PS} to construct the γ–X_{PS} "phase diagram" for PCL/PS blends as Langmuir films. In bulk, this blend exhibits an upper critical solution temperature (UCST) phase diagram. For the molar masses used here, $\phi_{critical}$ would occur at $\phi_{PS} \sim 0.80$. At the A/W interface, a higher Π is like a smaller T on a classical T-ϕ diagram. Here, using $\gamma = \gamma_0 - \Pi$ allows us to obtain a "UCST" type phase diagram. The tentative UCST type "phase diagram" for PCL/liquid PS oligomer blends is shown in Figure 9.10. Our preliminary study of the phase diagram for polymer blends as Langmuir films at the A/W interface represents the first such study to apply traditional concepts of phase diagrams to a 2D polymeric Langmuir monolayer. More detailed

studies of this subject will allow one to obtain a better understanding of the phase behavior of polymer blends in 2D thin film geometries.

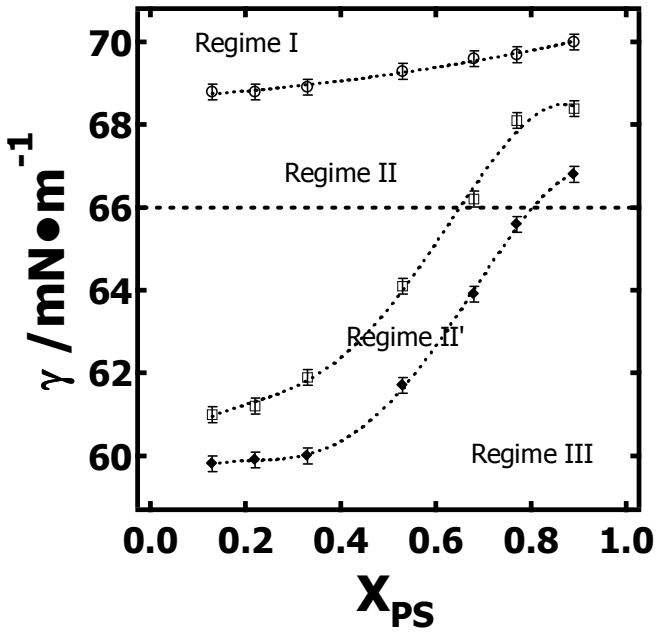

Figure 9.10. Critical γ values listed in Table 9.2 are plotted as a function of X_{PS} for various PCL (M_w = 10 kg•mol^{-1})/liquid PS oligomer (M_w = 0.74 kg•mol^{-1}) blends. Symbols correspond to (○) γ_a, (□) γ_b, and (♦) γ_c. Dotted lines represent the lines to guide the eyes. Regime I through III correspond to stable monolayer regime (I), metastable regime (II, II'), and unstable regime (III), respectively. The dashed line represents γ_{PCL} values from Table 9.2 and their extrapolation into Regime II and Regime III.

Surface morphologies for a PS-rich blend (X_{PS} ~ 0.89) for the PCL/liquid PS oligomer system are shown in Figure 9.11 to provide morphological support for the regimes of the tentative phase diagram in Figure 9.10 derived from Π-<A> measurements. For X_{PS} ~ 0.89 blends, PCL crystallization is inhibited. BAM images captured during dynamic

compression demonstrate homogeneous surface morphologies in Regime I as seen in Figure 9.11A. Further compression of the blend films into Regime II yields heterogeneously homogeneous surface morphologies with finely dispersed structures that can be seen in BAM (Figure 9.11B and C). BAM images captured in Regime II' show the growth of small droplets, presumably corresponding to phase separation by a nucleation and growth (NG) mechanism (Figure 9.11D through G). In regime III, small droplets give way to surface morphologies that are reminiscent of spinodal decomposition (Figure 9.11H and I). In highly PS-rich blends, the morphological features are consistent with the proposed phase diagram in Figure 9.10.

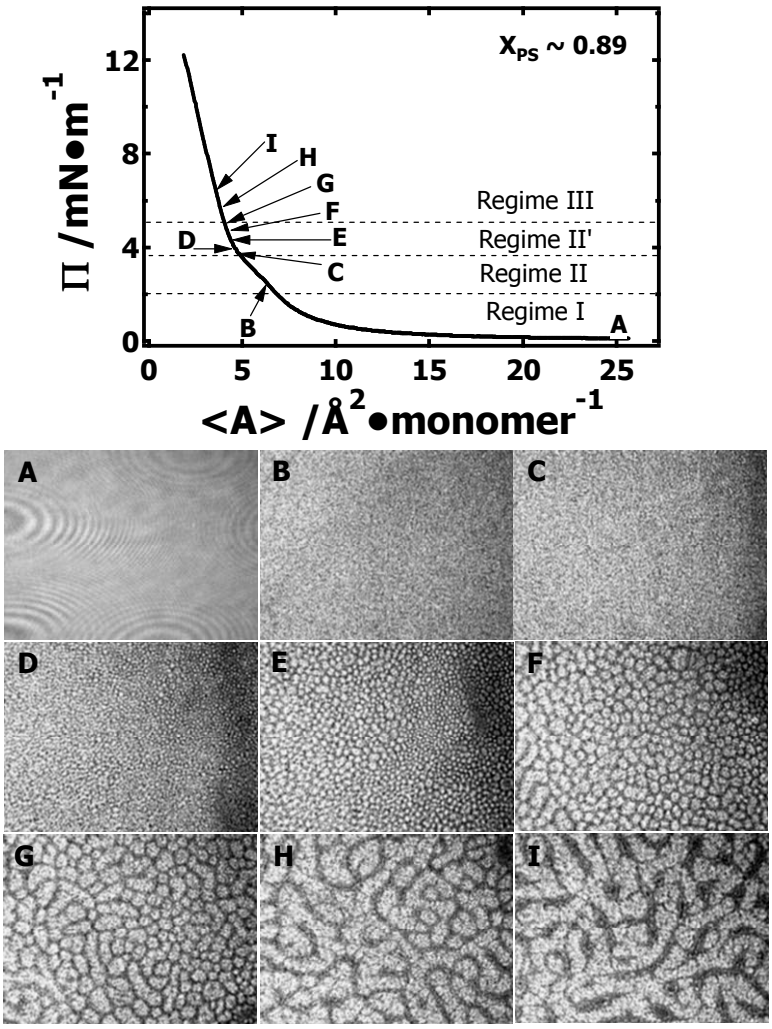

Figure 9.11. BAM images for a X_{PS} ~ 0.89 PCL (M_w = 10 kg•mol^{-1})/liquid PS oligomer (M_w = 0.74 kg•mol^{-1}) blend obtained at T = 22.5 °C and a compression rate of 20 cm^2·min^{-1} during the 1st compression step. The letters on the Π–<A> compression isotherm indicate where the individual BAM images (3.2 × 2.4 mm^2) were taken and correspond to (Image, <A>/Å^2·monomer^{-1}): (A, 25), (B, 6.4), (C, 4.9), (D, 4.6), (E, 4.4), (F, 4.2), (G, 4.1), (H, 3.8), and (I, 3.6). The horizontal dashed lines are different regimes identified through an analysis of ε_s: (I) stable monolayer regime, (II, II') metastable regimes, and (III) unstable regime as shown in Figure 9.10.

For the case of PCL-rich blends, complications in the phase diagram are expected. The reason for this expectation is bulk studies by Nishi *et al.*, where the crystallization of PCL makes it difficult to accurately determine the binodal line.[85-89] In other words, the binodal line below the melting point curve is ill-defined. With this in mind, a $X_{PS} \sim 0.33$ PCL (M_w = 10 kg•mol^{-1})/liquid PS oligomer (M_w = 0.74 kg•mol^{-1}) blend was examined by BAM and results are provided in Figure 9.12. As seen in Figure 9.12, bright spots in images F through I correspond to the nucleation and growth of PCL crystals. The crystallization process of PCL clearly takes place in the presence of phase separation. In spite of the complications that crystallization can cause, Regime II and Regime II' show morphologies (Figure 9.12A through C) that are consistent with the behavior seen in Figure 9.11 for PS-rich blends. One significant difference between the PS-rich and PCL-rich blends is a shift for spinodal-like morphological features into Regime II' for PCL-rich blends (Figure 9.12D through G) vs. Regime III for PS-rich blends. While the morphologies in Regime III differ for PS-rich (Figure 9.11G through I) and PCL-rich blends (Figure 9.12H and I), there is still a morphological change going from Regime II' to Regime III. For future work, additional morphological studies for PCL-rich blends are required to clarify the morphological transitions in the metastable regimes. We have also noted that both crystallization and phase separation are strongly compression rate dependent. As a suggestion for future work, dynamic compression experiments performed at different compression rates could be very interesting.

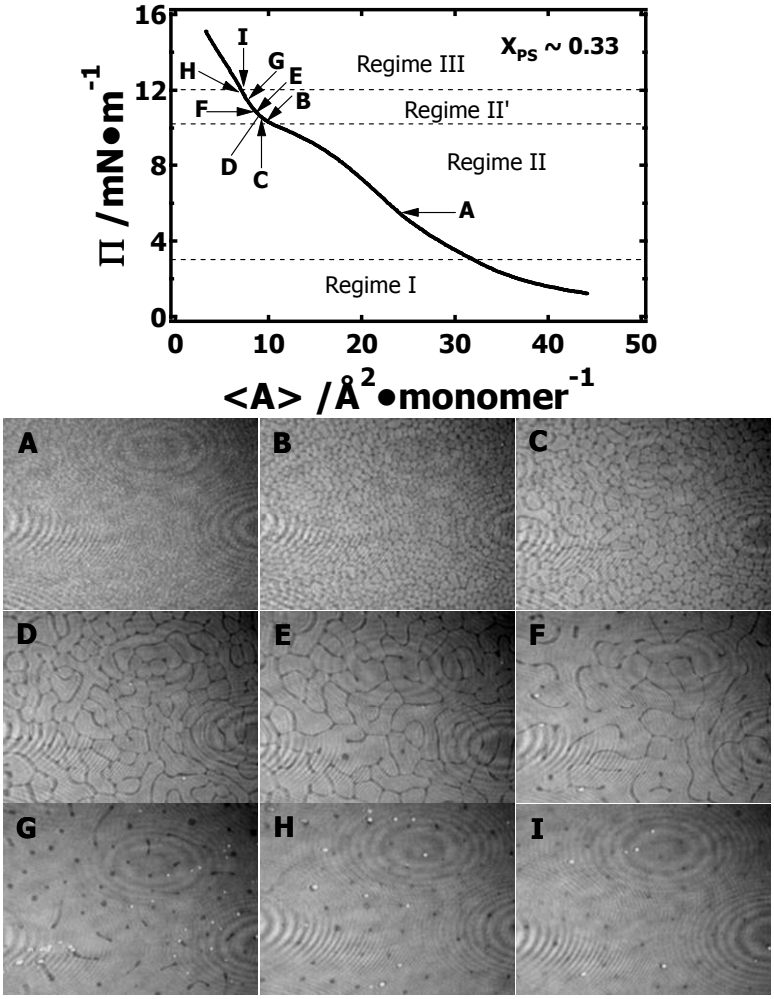

Figure 9.12. BAM images for a X_{PS} ~ 0.33 PCL (M_w = 10 kg•mol^{-1})/liquid PS oligomer (M_w = 0.74 kg•mol^{-1}) blend obtained at T = 22.5 °C and a compression rate of 20 cm^2·min^{-1} during the 1st compression step. The letters on the Π–<A> compression isotherm indicate where the individual BAM images (3.2 × 2.4 mm^2) were taken and correspond to (Image, <A>/Å^2·monomer^{-1}): (A, 24), (B, 9.7), (C, 9.4), (D, 8.9), (E, 8.7), (F, 8.4), (G, 7.8), (H, 7.2), and (I, 6.9). Bright domains in images F→I are PCL crystallites. The horizontal dashed lines are different regimes identified through analysis of ε_s: (I) stable monolayer regime, (II, II') metastable regimes, and (III) unstable regime as shown in Figure 9.10.

Another way to probe the proposed phase diagram in Figure 9.10 for PCL (M_w = 10 kg•mol^{-1})/liquid PS oligomer (M_w = 0.74 kg•mol^{-1}) blends as Langmuir films is isobaric area relaxation experiments in different regimes, particularly in the two metastable regimes (Regime II and II'). Interesting BAM images captured for a representative X_{PS} ~ 0.13 PCL/liquid PS oligomer blend during isobaric relaxation experiments at Π ~ 10 mN·m^{-1} are shown in Figure 9.13. These BAM images provide clear evidence for PCL/liquid PS oligomer phase separation proceeding simultaneously with the nucleation and growth of PCL crystals. In comparison with PCL/PtBA blends in Chapters 5 and 6, PCL crystals grown in PCL/liquid PS oligomer blends do not show dendritic sidebranches. This observation may arise from relatively fast diffusion of the PS oligomer in the blend films during the compression process. Another interesting feature of the BAM images in Figure 9.13 is that the growth fronts of the PCL crystals are essentially located at the interface between PCL and PS-rich phase separated domains. More detailed isobaric area relaxation experiments will allow one to explore the morphological evolution of PCL/liquid PS oligomer blends in different regimes with systems containing different PCL and PS molar masses, block copolymers, etc. at different temperatures.

Overall, the experimental results for PCL-based polymers as Langmuir films obtained thus far open the door to a wide range of future studies for polymers confined to 2D geometries. More efforts need to be made to gain a complete understanding of various PCL-based polymer blend systems as Langmuir films at the A/W interface.

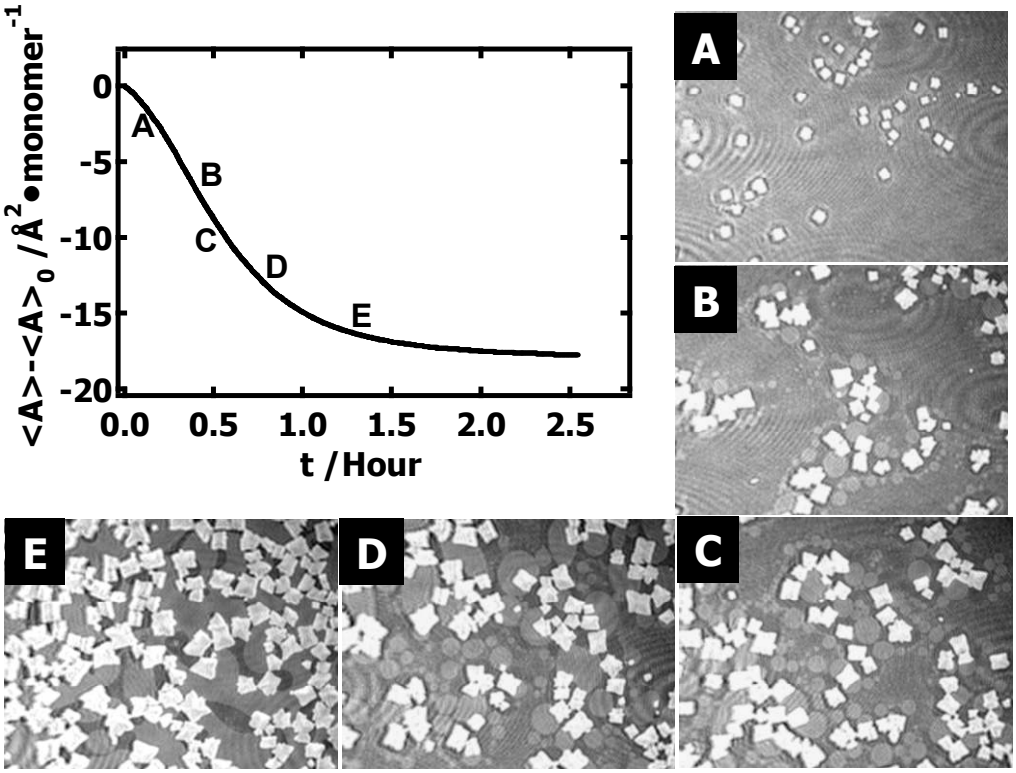

Figure 9.13. BAM images for a representative $X_{PS} \sim 0.13$ (M_w = 10 kg•mol^{-1})/liquid PS oligomer (M_w = 0.74 kg•mol^{-1}) blend obtained during isobaric area relaxation experiments at $\Pi \sim 10$ mN·m^{-1}. BAM images were taken during the isobaric experiments at different times: (A) 0.14, (B) 0.35, (C) 0.53, (D) 0.70, and (E) 1.15 h. Solid-like domains appear bright in all of the 3.2 × 2.4 mm^2 BAM images. Lighter gray domains indicate phases rich in liquid PS oligomer.